This document is the Accepted Manuscript version of a Published Work that appeared in final form in Nanoscale, 2015, 7, 7692. DOI: 10.1039/c5nr01037c

Efficient bulk heterojunction solar cells based on solution processed small molecules based on the same benzo[1,2-*b*:4, 5-*b*′]thiophene unit as core donor and different terminal units

Challuri Vijay Kumar [a], **Lydia Cabau** [a], **Emmanuel N. Koukaras** [bc], **Shahbaz A. Siddiqui** [d], **Ganesh D. Sharma** *[d] **and Emilio Palomares** *[ae]

[a]*Institute of Chemical Research of Catalonia (ICIQ), Avda. Països Catalans 16, E-43007 Tarragona, Spain*

[b]*Institute of Chemical Engineering Sciences, Foundation for Research & Technology, Hellas, Stadiou Str. Platani, Patras, 26504, Greece*

[c]*Molecular Engineering Laboratory, Department of Physics, University of Patras, Patras, 26500 GR, Greece*

[d]*R & D Center for Engineering and Science, JEC group of Colleges, Jaipur Engineering College, Kukas, Jaipur 303101, India. E-mail: gdsharma273@gmail.com;sharmagd_in@yahoo.com*

[e]*Catalan Institution for Research and Advance Studies (ICREA), Avda. Lluis Companys 23, E-08010 Barcelona, Spain. E-mail: epalomares@iciq.es*

We report the synthesis, characterization, and optical and electrochemical of properties of two novel molecules **DRT3-BDT (1)** and **DTT3-BDT (2)**, comprising the same BDT central core (donor) and different end capped acceptor units, *i.e.* rhodanine with ethyl hexyl and thiazolidione with ethylhexyl, respectively, linked *via* an alkyl-substituted terthiophene (3 T) π-conjugation bridge. The electrochemical properties of these small molecules indicate that their energy levels are compatible with energy levels of $PC_{71}BM$ for efficient exciton dissociation. These molecules have been used as electron donors along with $PC_{71}BM$ as an electron acceptor, for the fabrication of solution processed "small molecule" bulk heterojunction (BHJ) solar cells (smOPV). The device prepared from optimized **1** : $PC_{71}BM$(1 : 1) processed cast from

DIO (3%v)/CF solvent exhibited a power conversion efficiency of 6.76% with J_{sc} = 11.92 mA cm^{-2}, V_{oc} = 0.90 and FF = 0.63. The device with **2** : $PC_{71}BM$ under the same conditions showed a lower PCE of 5.25% with J_{sc} = 10.52 mA cm^{-2}, V_{oc} = 0.86 and FF = 0.56. The AFM, TEM and PL quenching measurements revealed that the high $J_{sc}$is a result of the appropriate morphology and exciton dissociation. The performances were compared for the devices based on two small molecules. The higher J_{sc} for device **1** was attributed to its better nanoscale phase separation, smooth surface and higher carrier mobility in the **1** : $PC_{71}BM$ blend film. Moreover, the higher value of FF for the **1** : $PC_{71}BM$ based device was ascribed to a good balance between the electron and hole mobilities.

1. Introduction

Over the last two decades, organic solar cells based on the bulk heterojunction (BHJ) active layer have drawn a lot of attention because of their advantages in weight, flexibility and simple manufacture, and are a promising technology for future energy harvesting.[1–7] Polymer based donor materials are one of the important components in organic BHJ solar cells,[8–13] where they have been used as a donor along with fullerene as an acceptor in the active layer, and a power conversion efficiency (PCE) over 9% has been reported.[14–18] The so-called "small molecule" based donor materials are an interesting alternative, offering several promising advantages over their polymer counterparts, including monodispersity and well defined molecular structure, easy purification, and better reproducibility (less batch to batch variation)[19–25] and a PCE in the range 8–10% has been achieved in recent years for single junction solar cells,[26–28] as well as a PCE of 10.1% for tandem cell devices.[29]

In most of the BHJ organic solar cells based on a solution processed small molecule as the donor, a relatively low fill factor (FF) and short circuit current (J_{sc}) were seen as compared to their polymer counterparts, due to their poorer film formation ability.[30] At present, different kinds of solution processed small molecules with wide absorption, high hole mobility, and appropriate miscibility, with a fullerene derivative acceptor to form uniform interpenetrating networks, have been developed for high efficiency small molecule BHJ solar cells. In particular, the most promising small molecule donor materials for BHJ solar cells are normally designed by connecting various electron donating (D) and electron withdrawing (A) moieties through a π-conjugating spacer *i.e.* (D–π–A) structure.[31–37] Such a D–π–A structure can be used to lower the optical bandgap to broaden the optical absorption profile and to assist the formation of favorable morphologies for efficient small molecule BHJ organic solar cells. Among the different small molecules with A–D–A structure for organic solar cells, benzo[1,2-*b*:4,5-*b*′]-dithiophene (BDT) derivatives have proved to be promising materials for photovoltaic applications.[38–40] The incorporation of thiophene side chains could extend the vertical π–π conjugation and promote π–π stacking in the solid state,[41,42] thereby

improving the charge transport, leading to an enhancement in the corresponding J_{sc}.[43] In the case of 2D BDT based polymer solar cells, high V_{oc} was demonstrated as compared to its one dimensional (1D) BDT counterparts, due to its deeper highest occupied molecular orbital (HOMO) energy levels,[44,45] and excellent photovoltaic performance was shown, with PCEs of over 7%.[41,46] The BDT unit is a symmetric and coplanar conjugated structure, and most importantly it can be relatively easily modified and exhibits good electron delocalization and excellent hole mobility. Chen and coworkers reported a 2D BDT small molecule, DR3TBDT, that demonstrated a PCE of 8.12%.[21] Recently, Chen *et al.* designed and synthesized a new A–D–A small molecule with BDT as the central donor core, namely DR3TSBDT for solution processed BHJ organic solar cells, and achieved a record PCE of 9.95%.[28] These research works also revealed that the nature of the acceptor end group mainly influences the performance of the resulting SMOPV. Hence, to enhance light absorption and tune the HOMO energy level, a lot of effort has been put into designing the new acceptor units.

A small molecule featuring an electron donating central core, π-conjugated spacers, and electron accepting end caps could be suitable for the preparation of the solution processed organic solar cells. In such systems, cyanoacetate and rhodanine acceptors have been employed in conjunction with different central donor cores, including benzodithiophene,[47,48]dithienosiole[49,50] and benzotriphiophene.[51] Chen *et al.* have recently designed a small molecule containing 4,8-dioctyl benzo[1,2-*b*:4,5-*b*′]dithiophene as the central block and 3-(2-ethylhexyl)-rhodanine as the end-capping groups and achieved a PCE of 8.26% through the active layer optimization process combining thermal and solvent vapor optimization.[52] Sun *et al.*have designed a new small molecule donor benzodithiophene terthiophene rhodanine (BTR) and achieved a excellent PCE of 9.3%.[53]

Recently, we have designed as small molecule with a BDT donor core and 3-ethylrhodanine as electron withdrawing end groups linked through a cyclopentadithiophene π spacer, and used it as a donor component along with $PC_{71}BM$ as the acceptor component for solution processed BHJ solar cells; we achieved a PCE of 6.07% after optimization of the solvent additive.[54] In continuation of our research work on the designing of new novel small molecules based on a BDT core, in this study, we have synthesized two A–D–A small molecules, denoted as **DRT3-BDT (1)** and **DTT3-BDT (2)**, comprising the same BDT as the central core (donor) and different end capped acceptor units, *i.e.* rhodanine with ethyl hexyl and thiazolidione with ethylhexyl linked *via* an alkyl-substituted terthiophene (3 T) π-conjugation bridge. These small molecules were used as the donor along with a $PC_{71}BM$ acceptor for the fabrication of solution processed small molecule BHJ organic solar cells. The devices, based on **1** :

$PC_{71}BM$ (1 : 1) and **2** : $PC_{71}BM$ (1 : 1), processed with DIO (3%v)/CF, exhibit PCE values of 6.76% and 5.26%, respectively.

2. Experimental details

2.1 Synthesis and characterization of small molecules

The synthesis of small molecules 1 and 2 and their detailed characterizations were given in the ESI.

2.2 Device fabrication and characterization

The small molecule BHJ solar cells were prepared as follows: First the ITO coated glass substrate was cleaned using detergent powder, acetone and isopropyl alcohol with ultra-sonication. After drying the cleaned ITO substrate in ambient atmosphere, the hole transport material of PEDOT:PSS (Clevious PH) was spin-coated at 3000 rpm for 40 s to obtain a film thickness of 40 nm. The **1** or **2** : $PC_{71}BM$ (donor : acceptor) blend solution was prepared from different weight ratios of 1 : 0.5, 1 : 1 and 1 : 1.5 and a total concentration of 20 mg mL^{-1} in chloroform (CF) with 1, 2, 3 and 4 v% of 1,8-diiodooctane (DIO) processing additive. After stirring overnight at 50 °C, the blend was heated to 80° C for 15 min before spin casting. The photoactive layer was obtained from spin casting the solution at 2000–2500 rpm for 60 min and then the film was dried at 60° C for 10 min to evaporate the residual solvent. The thickness of the active layer was controlled by the spinning speed during the spin coating of the active layer and was in the range 90–100 nm. Finally, the aluminum (Al) top electrode was thermally deposited on the active layer at a vacuum of 10^{-5} Torr through a shadow mask of area 20 mm^2. All devices were fabricated and tested in ambient atmosphere without encapsulation. The hole-only and electron-only devices with ITO/PEODT:PSS/**1** or **2** : $PC_{71}BM$/Au and ITO/Al/**1** or **2** : $PC_{71}BM$/Al architectures were also fabricated in an analogous way, in order to measure the hole and electron mobilities, respectively. The current–voltage characteristics of the BHJ organic solar cells were measured using a computer controlled Keithley 238 source meter under simulated AM1.5G, 100 mW cm^{-2}. A xenon light source coupled with an optical filter was used to give the stimulated irradiance at the surface of the devices. The incident photon to current efficiency (IPCE) of the devices was measured, illuminating the device through the light source and monochromator, and the resulting current was measured using a Keithley electrometer under short circuit conditions.

3. Results and discussion

3.1 Synthesis and characterization of small molecules

The chemical structures of **DRT3-BDT (1)** and **DTT3-BDT (2)** are shown in Scheme 1. The synthetic routes for two new small molecules **DRT3-BDT (1)** and **DTT3-BDT (2)**, based on benzodithiophene with different end group acceptors, are shown in Scheme 2. **DRT3-BDT (1)** and **DTT3-BDT (2)** consist of 5″,5‴″-(4,8-bis (5-(2-ethylhexyl)thiophen-2-yl) benzo [1,2-*b*:4,5-*b*′] dithiophene-2,6-diyl) bis (3,3″-dioctyl-

[2,2′:5′,2″-terthiophene]-5-carbaldehyde) (**7**) as the donor and 3-ethyl hexyl rhodanine and 3-ethylhexyl thiazolidine-2,4-dione with octyl terthiophene as a bridge. The BDT (**7**) building block was synthesized according to the reported procedure.[21] These two acceptors, synthesized *via* the potassium salts of rhodanine and thiazolidine-2,4-dione, reacted with ethylhexyl bromide in the presence of potassium iodide, with solvents of acetone and DMF. The targeted molecules were prepared by the Knoevenagel condensation with BDT (**7**), with 3-ethyl hexyl rhodanine and 3-ethylhexyl thiazolidine-2,4-dione, respectively. To obtain the best possible performance in OSC devices, **DRT3-BDT (1)**and **DTT3-BDT (2)** were purified by consecutive flash chromatography and size exclusion chromatography. This combination of techniques was found to be effective for removing most of the impurities. Both the small molecules are soluble in common organic solvents. The important intermediates and targeted molecules were characterized by ^{1}H-NMR, C^{13}-NMR and MALDI-TOF and with elemental analysis (for detail see the ESI).

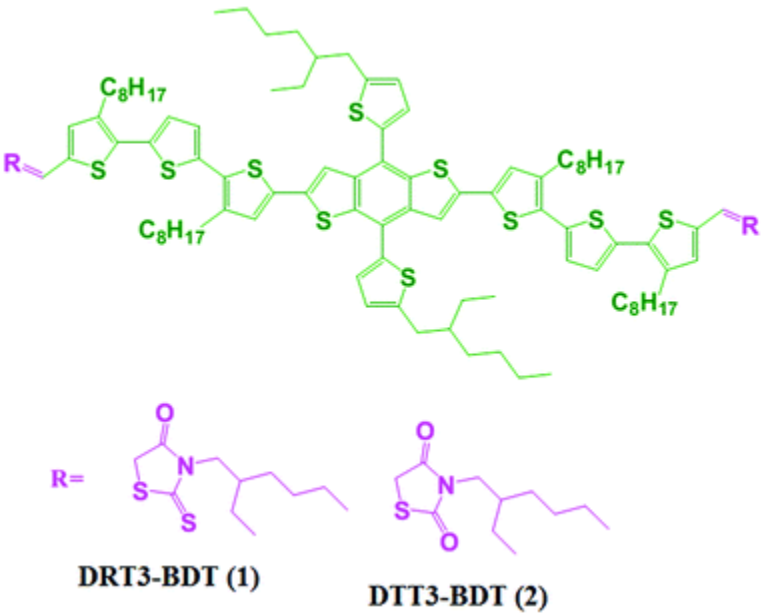

Scheme 1 Molecular structures of **DRT3-BDT (1)** and **DTT3-BDT (2)**.

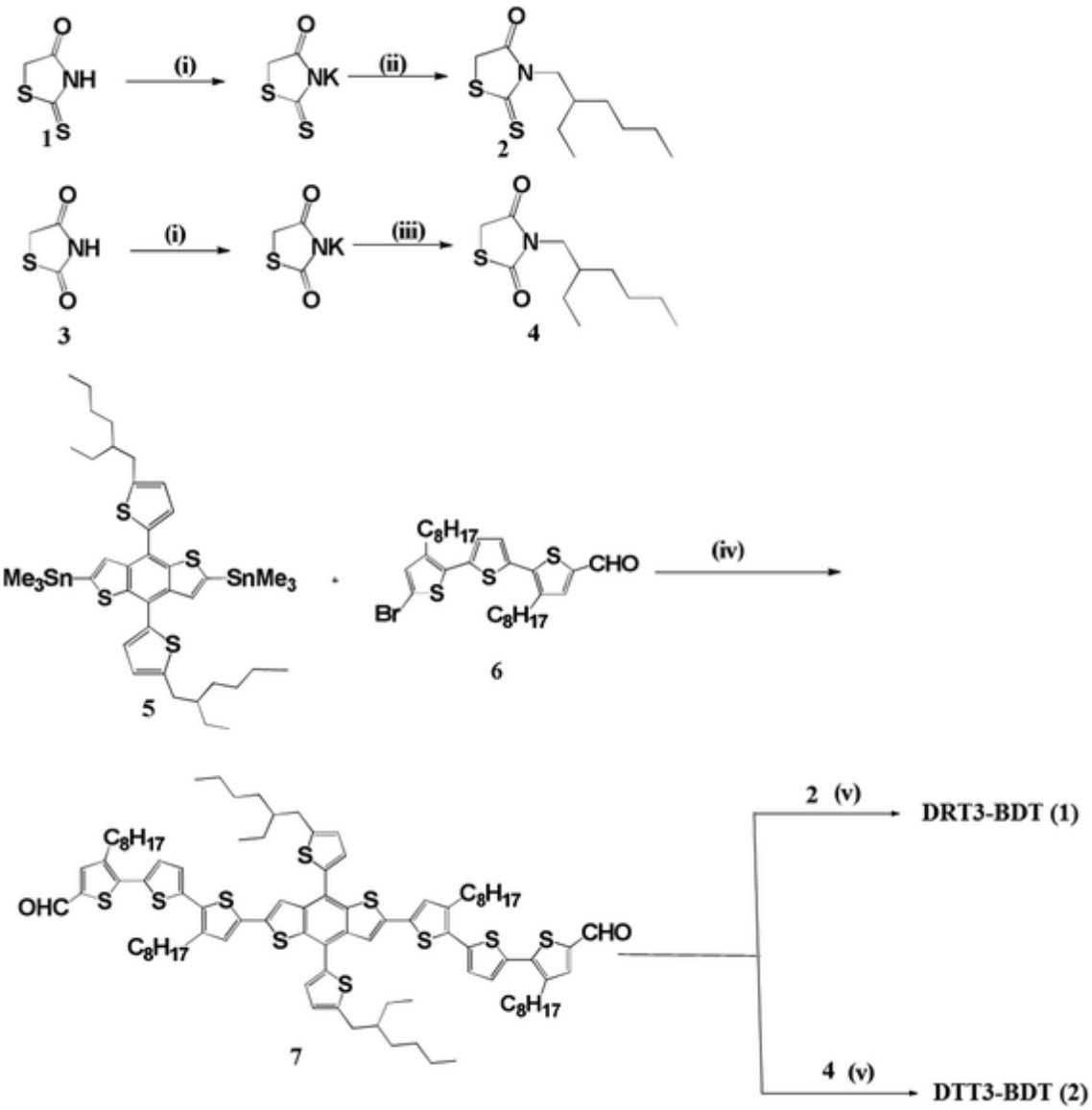

Scheme 2 Synthetic route of **DRT3-BDT (1)** and **DTT3-BDT (2)**. Reaction conditions: (i) KOH, ethanol, reflux, 5 h; (ii) ethyl hexyl bromide, KI, acetone, DMF, 36 h, 90° C; (iii) ethyl hexyl bromide, DMF, reflux, 4 h; (iv) dry toluene, $Pd(PPh_3)_4$, 110 °C, 48 h; (v) dry chloroform, piperidine reflux, 12–48 h.

3.2 Optical and electrochemical properties

Fig. 1a and b shows the absorption spectra of compounds in dilute chloroform solution and thin film cast from chloroform solvent, respectively. The absorption spectra of both small molecules in solution are identical and exhibit one main peak around 506 nm and 492 nm for **DRT3-BDT (1)** and **DTT3-BDT (2)**, respectively, which is attributed to the intramolecular charge transfer (ICT) between the donor and acceptor units present in the

small molecules; other smaller peaks at shorter wavelengths could be assigned to the π–π* transitions. As compared to the absorption spectra of these small molecules, the thin film, the spectrum was broadened and redshifted, with maximum absorption at wavelengths around 576 nm and 556 nm for **1** and **2**, respectively. In addition, a vibronic shoulder peak at 632 nm and 606 nm for **1** and **2**, respectively, was observed, which indicates effective π–π stacking between molecule backbones. The optical bandgap estimated from the onset of absorption is around 1.74 eV and 1.84 eV for **1** and **2**, respectively.

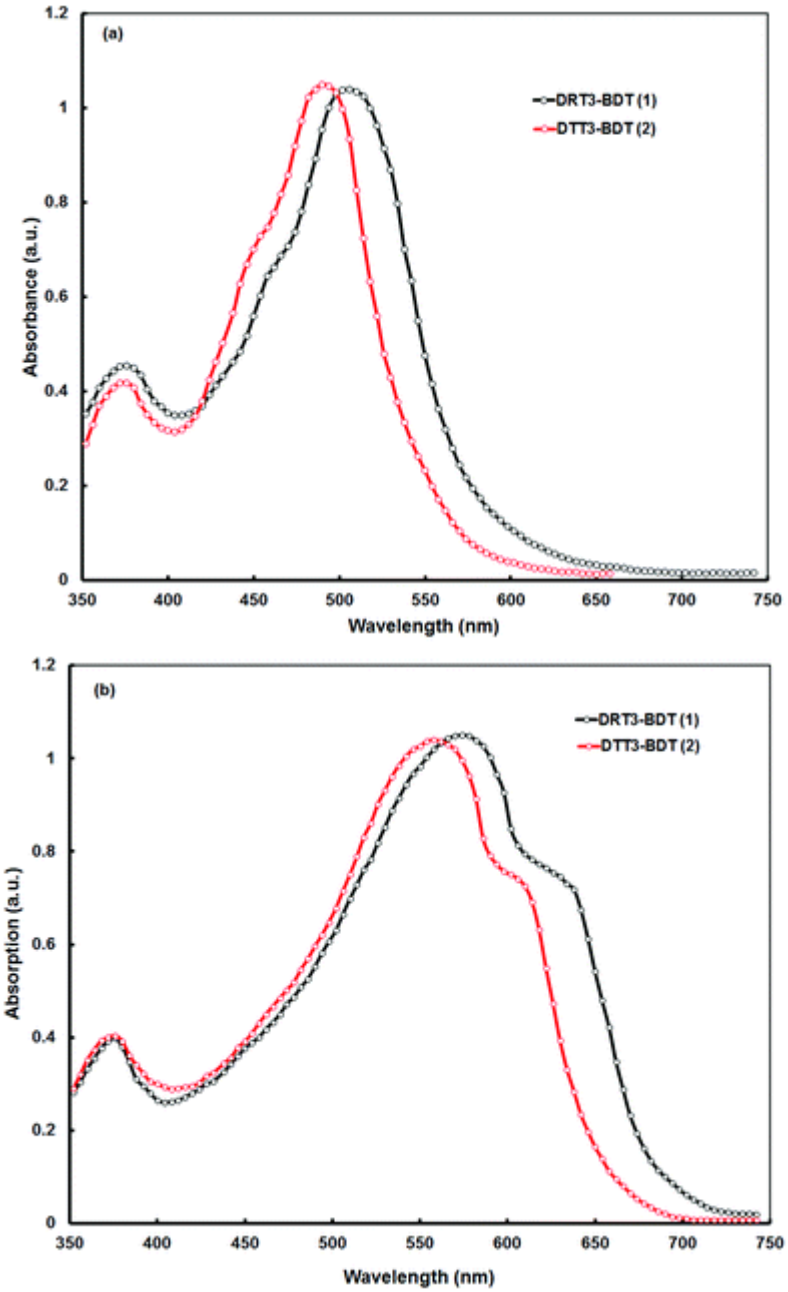

Fig. 1 Optical absorption spectra of **DRT3-BDT (1)** and **DTT3-BDT (2)** in (a) chloroform solution and (b) thin film cast from chloroform solution.

Cyclic voltammetry (as shown in Fig. 2a and b) was used to estimate the HOMO and LUMO energy levels of the small molecules. The potentials were internally calibrated using the ferrocene/ferrocenium (Fc/Fc^{+}) redox couple (4.4 eV below the vacuum level). The estimated values of the HOMO and LUMO energy levels are compiled in Table 1. The HOMO levels of both the small molecules are the same (−5.42 eV and −5.38 eV for **1** and **2**) but the LUMO levels are different (−3.54 eV and −3.44 eV, respectively), which is attributed to having the same core donor (BDT) and different acceptors in the small molecules, since the HOMO energy level in the D–A molecule depends upon the donor, while the LUMO energy level is decided by the type of acceptor. The electrochemical bandgap is estimated to be about 1.88 and 1.94 eV for **1** and **2**, respectively, which is in agreement with the optical bandgap. The deeper level of the HOMO in these small molecules could generate high values of V_{oc} in BHJ organic solar cells.

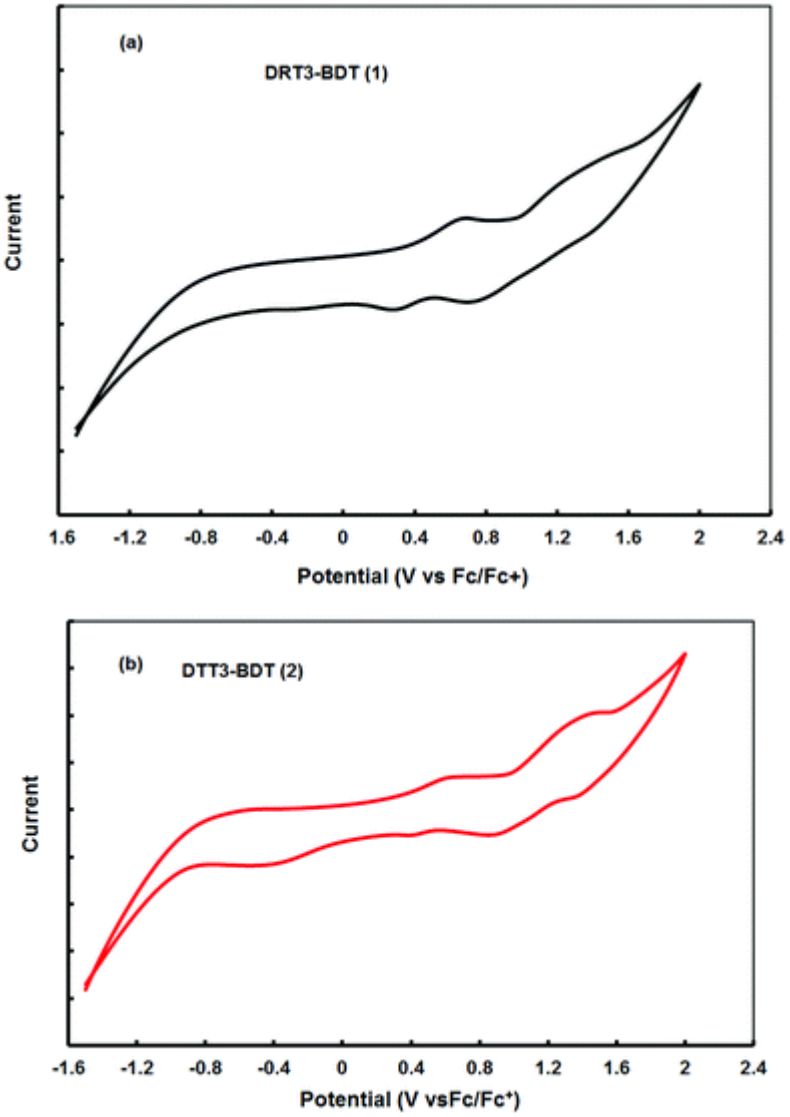

Fig. 2 Cyclic voltammetry of **DRT3-BDT (1)** and **DTT3-BDT (2)**.

Table 1 Calculated properties of **DRT3-BDT (1)** and **DTT3-BDT (2)** molecules. Specifically HOMO and LUMO energies (eV), HOMO–LUMO gap (eV), HL, optical gap (eV), OG, with corresponding oscillator strengths, *f*, the wavelengths and the main contributions to the first excited state, and the dipole moment (D), μ

	HOMO (eV)	LUMO (eV)	HL (eV)	OG (eV)	λ_{1st} (nm)	*f*	Main contributions	μ (D)
a **Values when solvent effects are taken into account for chloroform.**								
DRT3-BDT (1)								
PBE	−4.55	−3.40	1.15	1.25	990	0.95	H → L (91%), H − 1 → L + 1 (5%)	2.20
B3LYP	−5.11	−2.90	2.21	1.95	637	2.83	H → L (94%)	2.03
M06	−5.37	−2.80	2.58	2.09	592	3.63	H → L (81%), H−1 → L + 1 (10%), H → L + 2 (6%)	1.40
	−5.40[a]	−2.85[a]	2.54[a]	2.02[a]	613[a]	3.96[a]	H → L (77%), H−1 → L + 1 (13%), H → L + 2 (6%)[a]	1.77[a]
DTT3-BDT (2)								
PBE	−4.51	−3.28	1.23	1.36	914	1.00	H → L (89.8%), H − 1 → L + 1 (5%)	2.50
B3LYP	−5.10	−2.74	2.35	2.07	599	2.81	H → L (95%)	2.93
M06	−5.38	−2.65	2.74	2.22	558	3.33	H → L (82%), H − 1 → L + 1 (10%), H → L + 2 (5%)	3.11
	−5.42[a]	−2.69[a]	2.72[a]	2.16[a]	574[a]	3.68[a]	H → L (79%), H − 1 → L + 1 (12%), H → L + 2 (5%)[a]	3.60[a]

3.3 Theoretical calculations

We have additionally performed a theoretical study on the **1** and **2** molecular structures within the framework of density functional theory (DFT) and time-dependent density functional theory (TD-DFT). The initial geometry optimization calculations were performed, employing the gradient corrected functional PBE[55] of Perdew, Burke and Ernzerhof. The def-SVP basis set[56] was used for all of the calculations. At this stage of the calculations, to increase the computational efficiency (without loss of accuracy), the resolution of the identity method[57,58] was used for the treatment of the two-electron integrals. Subsequent geometry optimizations were further performed using the hybrid exchange–correlation functional B3LYP,[59] as well as Truhlar's meta-hybrid exchange–

correlation functional M06,[60] and the same basis set. Tight convergence criteria were placed for the SCF energy (up to 10^{-7} Eh) and the one-electron density (rms of the density matrix up to 10^{-8}), as well as for the norm of the Cartesian gradient (residual forces both average and maximum smaller than 1.5×10^{-5} a.u.) and residual displacements (both average and maximum smaller than 6×10^{-5} a.u.). Solvent effects were included for chloroform (CF), using the integral equation formalism variant of the Polarizable Continuum Model (IEFPCM), as implemented in the Gaussian package.[61]

TD-DFT excited state calculations were performed to calculate the optical gap of the **1** and **2** molecules using the same functionals and basis set on the corresponding ground state structures. The UV/Vis spectra were calculated using the B3LYP and M06 functionals. The first round of geometry optimization was performed using the Turbomole package.[62] All of the follow up calculations were performed using the Gaussian package.[61]

For the geometry optimization of the **1** molecular structure, several rotamers were examined as initial geometries, including aliphatic configurations. We performed vibrational analysis on the energetically lowest optimized structure and found it to be a true local (if not global) minimum; none of the vibrational modes had imaginary eigen frequencies. The two structures of lowest energy were suitably modified and used as initial geometries of the **2** structure for the corresponding geometry optimizations. In this case as well, vibrational analysis on the final, energetically lowest, structure revealed no imaginary eigenfrequencies. The backbone of the structures, *i.e.* the chain of ring units, is highly planar, with average dihedral angles between neighboring rings being around 12°. The dihedral angles between the edge thiazolidine-groups are in the range 11°–15° for **1** and 13°–17° for **2**, depending on the functional used and the presence of solvent. We have calculated the HOMO and LUMO energy levels and the optical gaps, defined here as the energetically lowest allowed vertical electronic excitation, employing the PBE, M06, and B3LYP functionals. In Table 1, in addition to the frontier orbitals' energy levels, we also provide the optical gap and the main contributions to the first excitation, as well as the wavelength of the first excitation and of the excitations with the largest oscillator strengths.

In addition to the B3LYP functional we have also performed our calculations employing the M06 functional. The M06 meta-hybrid functional was chosen, since it provides leveled performance over transition types.[62–64] We provide results using all three functionals, which can additionally be used for comparison with the literature.

We find, as expected, that the PBE functional underestimates both the HOMO–LUMO (HL) and the optical gaps. The HL gap calculated using the hybrid B3LYP functional is about 0.35 eV smaller than that using the meta-hybrid M06 functional, however, for the calculated optical gaps this difference is smaller, about 0.15 eV, with the latter being in better agreement with experimental values for the optical gap. In Table 1, we also provide the character of the first allowed excitations, only for

contributions larger than 4%. The first excitation, as calculated by the PBE and B3LYP functionals, exhibits a single-configuration character, while for the meta-hybrid functional M06 moderate secondary contributions are also noted.

In Fig. 3, we have plotted the isosurfaces (isovalue = 0.02) of the HOMO and LUMO, as well as the next nearest frontier orbitals that take part in transitions contributing to the first excitation, of the **1** and **2** structures. For both structures the HOMO extends over the main, nearly planar, body of the structures, with very small contributions from the edge thiazolidine- (**TAD** and **TADO**) groups. The LUMO on both structures seems to be localized on the terthiophene (**TT**) chains and the edge thiazolidine groups, with very small contributions from the central part (dithiophenylbenzodithiophene) (**DTBDT**) of the structures. This partitioning is even more pronounced for LUMO+1. For LUMO+2 this may seem reversed, since it is localized on both the central and edge part of the structures. However, by examining the contribution to the first excitation, the transition to LUMO+2 is from the HOMO, which displays greater localization in the central region. To quantify the contributions of the moieties to the frontier orbitals, we have calculated the total and partial density of states (PDOS). The PDOS for **1** and**2** is shown in Fig. 4. We partition **1** into the **TAD**, **TT**, **DTBDT**, and aliphatic groups. **2** is treated similarly, but instead of **TAD** we denote **TADO** for the -dione oxygens. For the **1** structure the contributions of the **BTBDT**, **TT**, and **TAD** groups to the HOMO are 39.7%, 53.2%, and 5.6% respectively, with only a 1.4% combined contribution from all the aliphatic groups. The corresponding contributions to the LUMO are 7.1%, 58.7% and 33.6%, respectively, and 0.6% combined from all the aliphatic groups. This is in agreement with our earlier observation on the localization of HOMO on the inner structure and the LUMO mainly on the outer structure. The first significant contributions (7.0%) from the aliphatic groups are noted at lower energies, around −7.4 eV, which correspond to the HOMO−13 level. For the **2** structure the contributions of the **BTBDT**, **TT**, and **TADO** groups to the HOMO are 42.8%, 51.0%, and 4.7% respectively, with only a 1.4% combined contribution from all the aliphatic groups. The corresponding contributions to the LUMO are 11.1%, 64.4% and 23.6%, respectively, and 0.8% combined from all the aliphatic groups. The first significant contributions (6.9%) from the aliphatic groups are noted at lower energies, around −7.52 eV, which corresponds to the HOMO−13 level.

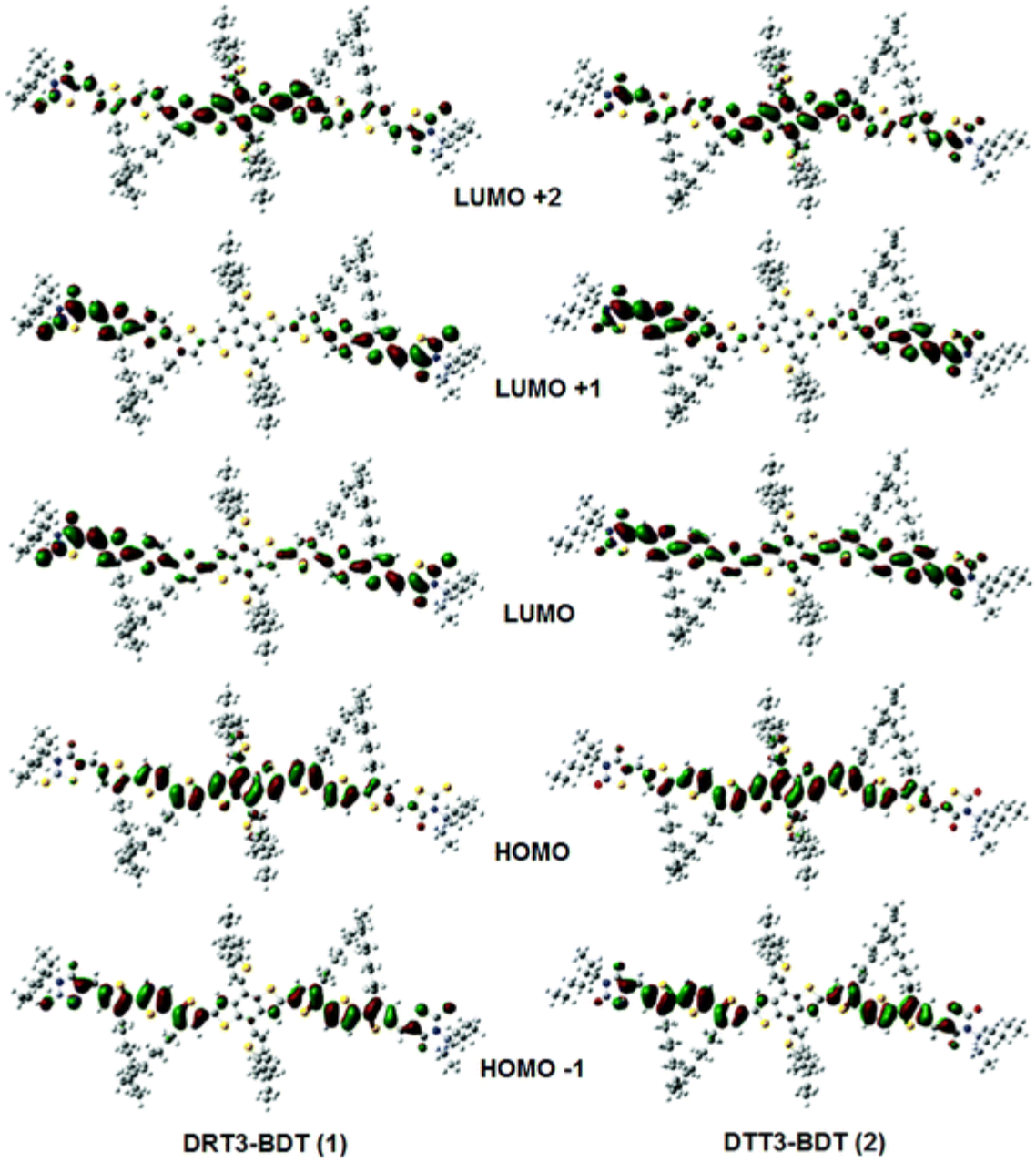

Fig. 3 Frontier and near frontier orbitals of the (left) **DRT3-BDT (1)** and (right) **DTT3-BDT (2)** molecules.

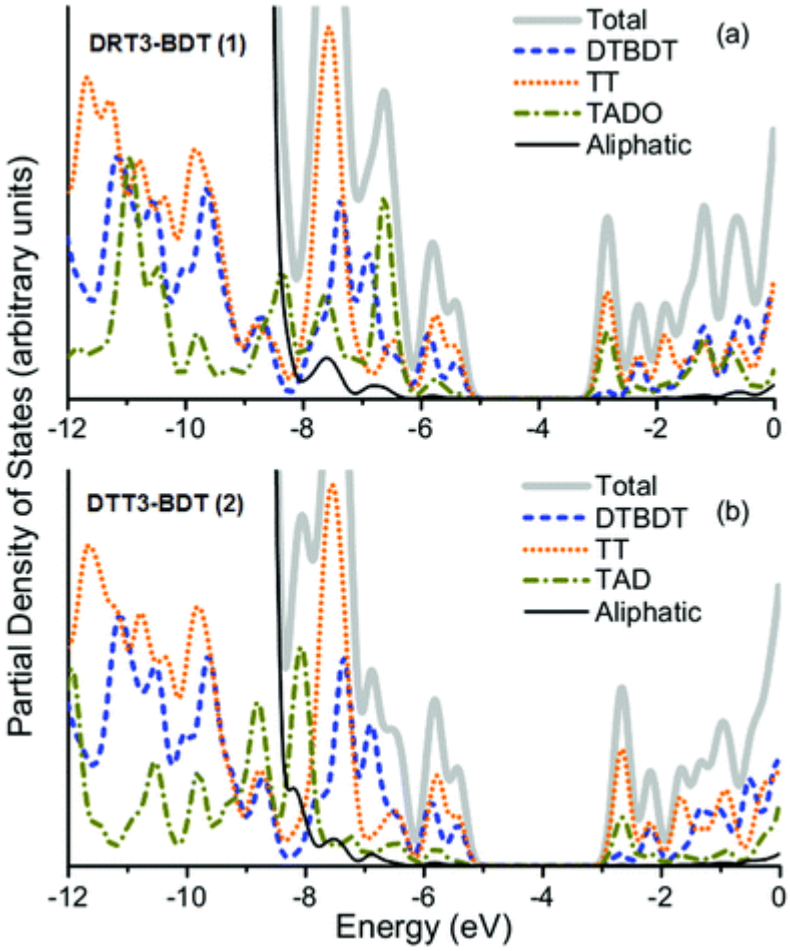

Fig. 4 Total and partial density of states of the (a) **DRT3-BDT (1)** and (b) **DTT3-BDT (2)**molecules (calculated using the M06 functional).

In Fig. 5, we show the UV/Visual absorption spectra of the **1** and **2** structures calculated at the TD-DFT/M06 level of theory, both accounting for solvent effects for CF and in the gas phase. The spectra have been produced by convoluting Gaussian functions with HWHM = 0.20 eV centered at the excitation wavenumbers. In Fig. S13 (see ESI†) we also provide the corresponding spectra calculated using the B3LYP functional, which has somewhat overestimated wavenumbers compared to both the spectrum calculated with M06 and the experimental spectrum. The low energy band calculated using M06 is overestimated by about 80 nm. The absorption spectra of both structures display three main bands in the visual region, which cover a wide spectral range.

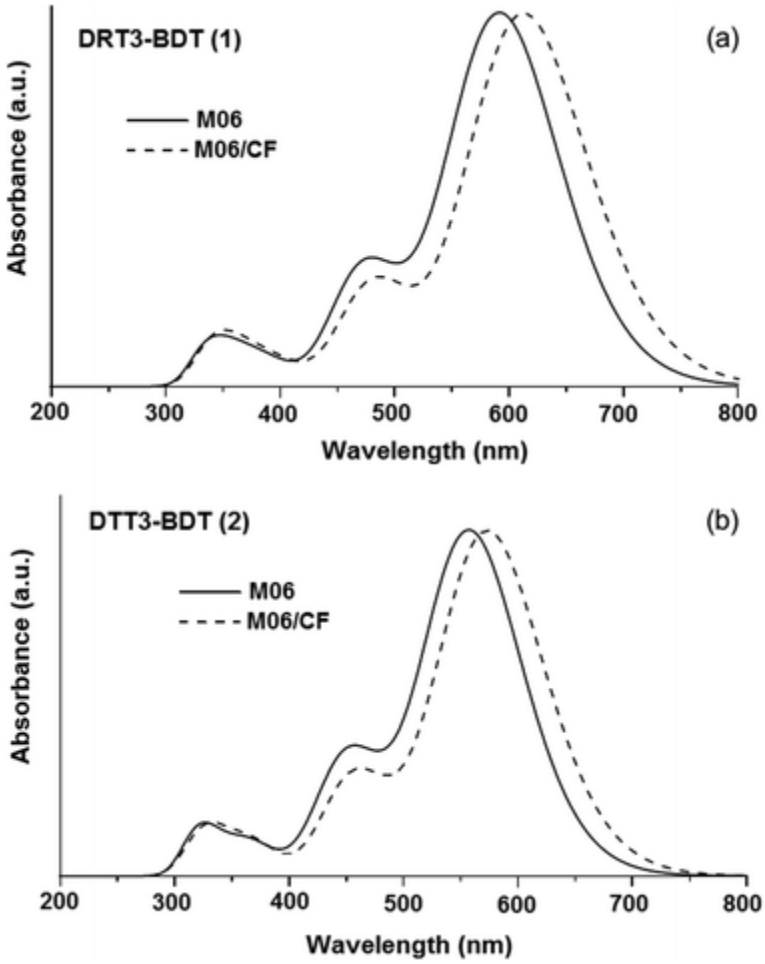

Fig. 5 Theoretical UV/Vis absorption spectra of (a) **DRT3-BDT (1)** and (b) **DTT3-BDT (2)**(calculated using the M06 functional).

A characteristic three band absorption spectrum is found, which displays a main band centered at 613 nm for **1** and 574 nm **2**, and two lower intensity bands at smaller wavelengths, specifically centered at 488 nm and 340 nm for **1**, and 445 nm and 324 nm for **2**. The calculated spectrum is slightly overestimated compared to the available region of the experimental one by about 75 nm. The wavelengths of the excitations with the largest oscillator strengths within these bands are given in Table 1.

Fig. 6 shows the absorption spectra of **1** : $PC_{71}BM$ and **2** : $PC_{71}BM$ blend (optimized ratio 1 : 1 for the best performance BHJ organic solar cells) thin films with and without DIO additives. The normalized absorption bands observed in **1** or **2** : $PC_{71}BM$ BHJ films without an additive exhibited spectral characteristics similar to that of their pristine solid state film, but the peak intensities of their vibronic shoulders were slightly decreased. However, these shoulder peaks reappear with the addition of additive,

indicating that the additive affected the intermolecular π–π packing interaction of these small molecules in the blend morphology.[65]

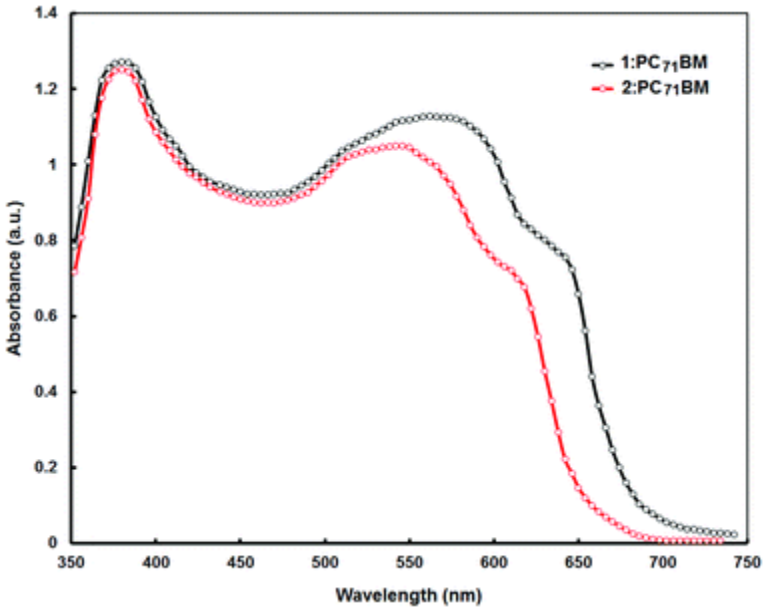

Fig. 6 Normalized UV-vis absorption spectra of the **1** or **2** : $PC_{71}BM$ (1 : 1) thin films cast from DIO/CF.

3.4 Photovoltaic properties

The organic solar cells were fabricated using the blends of these solution processed small molecules as electron donors, along with $PC_{71}BM$ as an acceptor, with a conventional device structure of ITO/PEDOT:PSS/**1** or **2** : $PC_{71}BM$/Al. First of all we have optimized the weight ratio of donor (**1** or **2**) to acceptor ($PC_{71}BM$) for the CF cast blend and found that the optimized ratio was 1 : 1. Then we have varied the solvent additive (DIO) concentration and found that the optimized volume ratio was 97 : 3 (CF/DIO). The **1** or **2** : $PC_{71}BM$ blends were dissolved in a optimized mixed solvent containing CF and 1,8-diiodoctane (DIO) in a volume ratio of 97 : 3. Devices prepared using either small molecule showed the best performances for a **1** or **2** : $PC_{71}BM$ blend ratio of 1 : 1. The best current–voltage (*J*–*V*) characteristics of the devices, under the illumination of AM1.5 G, 100 mW cm^{-2}, are displayed in Fig. 7a, and corresponding photovoltaic parameters are compiled in Table 2. With an optimized weight ratio of **1** or **2** to $PC_{71}BM$ at 1 : 1 (processed with 3%v DIO/CF), the device based on **1** : $PC_{71}BM$ showed a PCE of 6.76% with J_{sc} = 11.92 mA cm^{-2}, V_{oc} = 0.90 V and FF = 0.63. In contrast the device based on **2** : $PC_{71}BM$ showed a lower PCE of 5.25% with a J_{sc} = 10.52 mA cm^{-2}, V_{oc} = 0.86 V and FF = 0.58. The devices based on **1** and **2** displayed a

high V_{oc}, considering their deeper HOMO energy levels. The higher value of PCE for **1** : $PC_{71}BM$ when compared to **2** : $PC_{71}BM$, under identical conditions, is attributed to the larger value of J_{sc} and FF and is also consistent with the higher values of IPCE (Fig. 7b). The absorption spectrum (Fig. 6) of the blends clearly shows that the number of photons absorbed by **1** : $PC_{71}BM$ is higher than that of **2** : $PC_{71}BM$, resulting in higher J_{sc}. The higher value of FF for a device based on **1** as compared to **2** is attributed to a decrease in the series resistance (R_s), as measured from the slope of the forward *J–V* characteristics under illumination around the V_{oc}, and by an increase of shunt resistance (R_{sh}), as derived from the slope of *J–V* characteristics in the third quadrant.

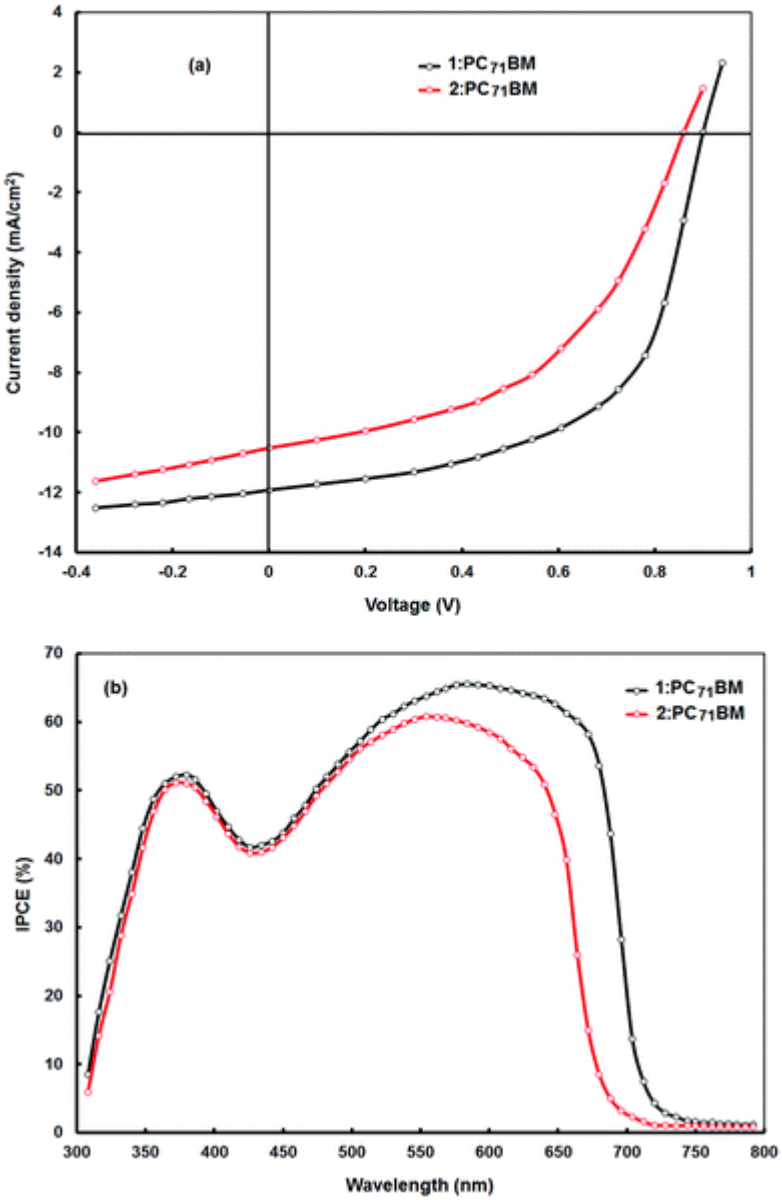

Fig. 7 (a) Current–voltage (*J–V*) characteristics under illumination and (b) IPCE spectra of BHJ small molecule solar cells using **1** or **2** : $PC_{71}BM$ processed with DIO/CF solvents.

Table 2 Photovoltaic parameters of devices

Blends	J_{sc} **(mA cm^{-2})**	V_{oc} **(V)**	**FF**	**PCE (%)**
1 : $PC_{71B}M$	11.92	0.90	0.63	6.76
2 : $PC_{71B}M$	10.52	0.86	0.58	5.25

The IPCE curves of the devices based on **1** and **2** are shown in Fig. 7b. The IPCE spectra closely resemble the absorption spectra of the corresponding layers. Clearly, both small molecules **1** and **2** contribute in the longer wavelength region and $PC_{71}BM$ contributes more in the shorter wavelength region. Under the same experimental conditions, IPCE values for the device based on **1** are higher than those for the device based on **2**, in good agreement with the larger value of J_{sc} for **1**. The higher values of J_{sc} and FF may also be attributed to the higher hole mobility for the **1** : $PC_{71}BM$ blend and the broader absorption profile of the **1** : $PC_{71}BM$ blend. The integrated values of J_{sc} from the IPCE spectra of the device based on **1** and **2** are 11.80 mA cm^{-2} and 10.42 mA cm^{-2}, respectively. These values are in agreement with the experimental values of J_{sc}.

It was reported that optimal BHJ morphologies consist of interpenetrating bicontinuous nanoscale domains (15–20 nm) of each donor and acceptor component, on the order of exciton diffusion length, which extend vertically from each electrode, thereby increasing the surface area D–A interface and forming continuous conducting pathways for efficient exciton dissociation, charge transfer and extraction.[66–70] To understand the information about the higher J_{sc} and FF for the device based on **1**, as compared to **2**, we have investigated the morphology of the active layers, exciton dissociation efficiency, and charge carrier mobilities in the small molecules and small molecule : $PC_{71}BM$ films. The film morphologies were investigated using TEM and AFM. The TEM images of the small molecule : $PC_{71}BM$ are shown in Fig. 8. Both the films showed a nanoscale phase separation, while the **1** : $PC_{71}BM$ blend exhibits more homogeneous nanoscale phase separation than that of **2** : $PC_{71}BM$. AFM images of small molecule : $PC_{71}BM$ blend films are shown in Fig. 9. AFM images of both the film showed smooth surfaces, while the roughness of the **1** : $PC_{71}BM$ film (rms = 1.25 nm) was lower than that for the **2** : $PC_{71}BM$ film (rms = 1.90 nm).

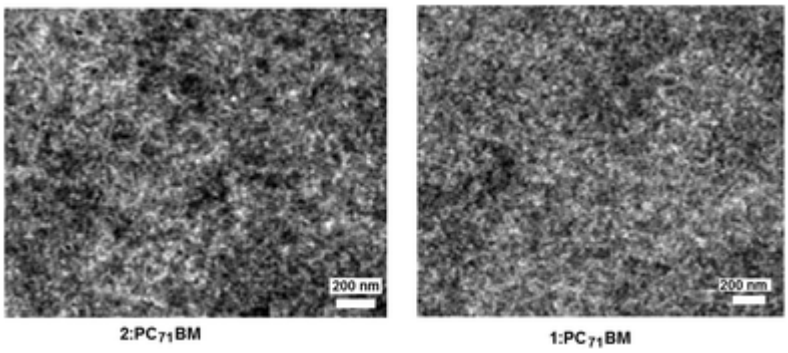

Fig. 8 TEM images of **1** : $PC_{71}BM$ and **2** : $PC_{71}BM$ cast from DIO·THF.

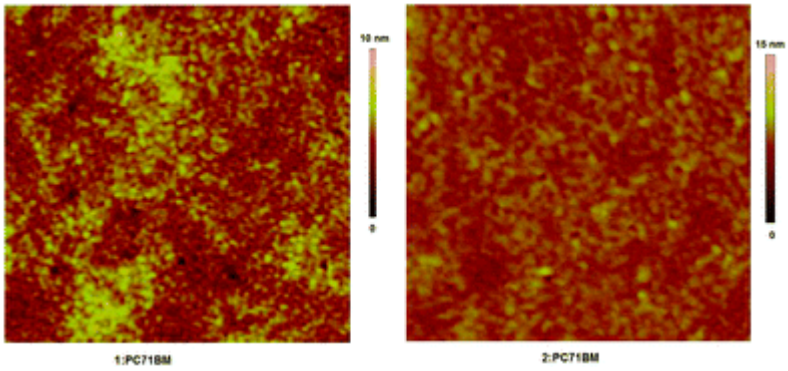

Fig. 9 AFM images of **1** : $PC_{71}BM$ and **2** : $PC_{71}BM$ cast from the DIO/CF solvent, image size 3μm × μm.

Photoluminescence (PL) spectra of pristine small molecules and their blends with PCBM thin films cast from THF and DIO/CF were measured to get more information about the exciton dissociation efficiency in the devices. Fig. 10 shows the PL spectra of small molecules and **1** or **2** : $PC_{71}BM$ blends spin cast from THF or DIO/CF solvents. **1** and **2** showed PL with peaks at around 618 nm and 708 nm, respectively. Blending upon $PC_{71}BM$ with a small molecule significantly quenched the PL. The quenching is more effective with the addition of DIO. This effective quenching indicates that the exciton dissociation was efficient in both blend films. More effective quenching in **1** : $PC_{71}BM$ than in the **2** : $PC_{71}BM$ blend could be attributed to two possibilities: (i) better exciton dissociation efficiency in the **1** : PCBM blend film and (ii) larger interfacial area between the small molecule and $PC_{71}BM$ through more optimal nanoscale phase separation. The former possibility may be possible because **1** had a higher LUMO energy level than **2**. The latter was mainly responsible for effective PL quenching, as confirmed from the morphological measurements. From the morphology and PL studies, we conclude that the **1** : $PC_{71}BM$ active layer has more favorable features for higher J_{sc}.

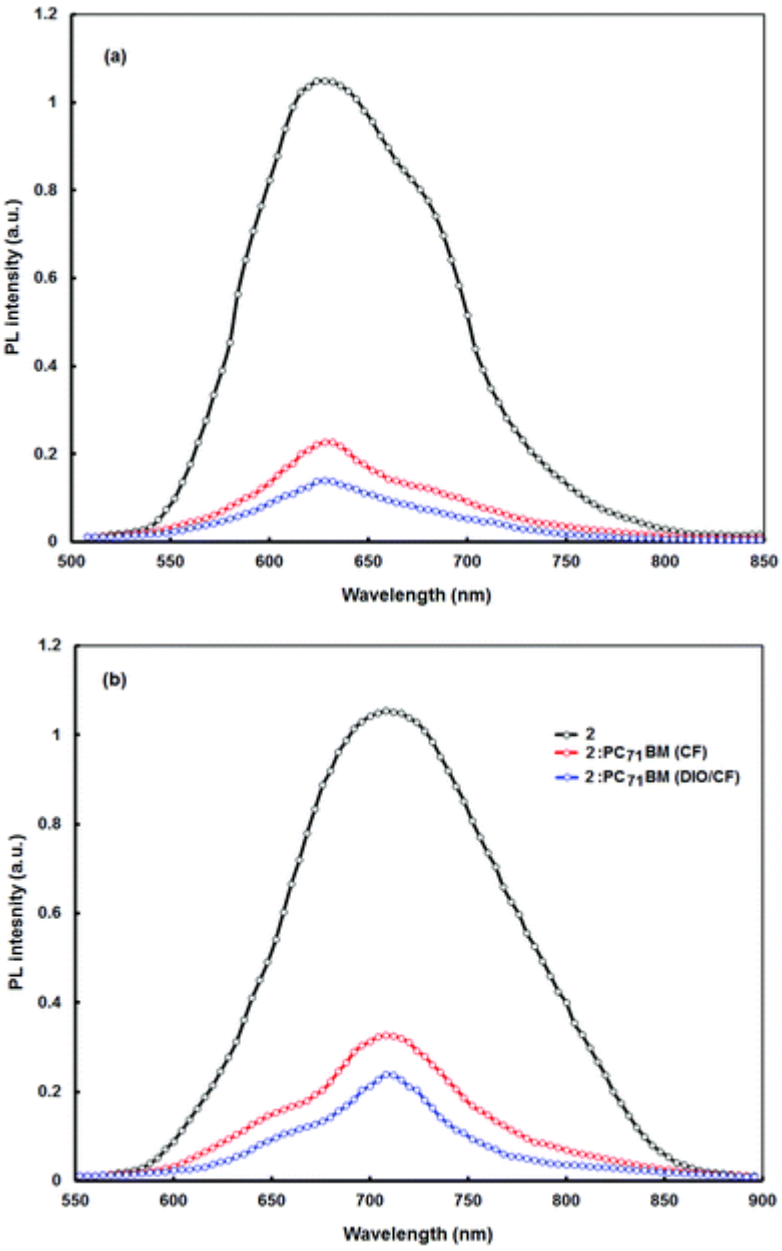

Fig. 10 (a) Photoluminescence spectra of (a) **1** and **1** : $PC_{71}BM$ films and (b) **2** and **2** : $PC_{71}BM$ films spin-coated from solution with or without the 3 vol% DIO additive.

The hole mobility is an another important factor for OSCs, because it influence the charge transport in the device. High hole mobility and balance between the electron and hole mobilities of BHJ active layer are necessary for effective charge carrier transport to the electrodes and also reduces photocurrent loss in the OSCs. The hole and electron mobilities were measured by a space charge limited current (SCLC) method with a

device structure of ITO/PEDOT:PSS/**1** or **2** : $PC_{71}BM$/Au (hole only) and ITO/Al/**1** or **2** : $PC_{71}BM$/Al (electron only), respectively. We have also measured the hole mobilities for pristine small molecules. The current density (JSCLC) in the SCLC region is described by the following expression:

$$J_{SCLC} = \frac{9}{8}\varepsilon_o \varepsilon_r \mu \frac{V^2}{L^3},$$

where ε_o is the permittivity of free space, ε_r is the relative dielectric constant of the transport medium, μ is the charge carrier mobility (hole and electron for hole only device and electron only device, respectively), $V = V_{appl} - V_{bi}$, (V_{appl} and V_{bi} are applied voltage and built in potential) is the internal potential in the device and L is the thickness of the active layer. The current–voltage characteristics for the hole-only devices in dark are shown in Fig. 11. As shown in Fig. 11, according to the above expression, the hole mobility was calculated to be 8.68×10^{-5} and 2.94×10^{-5} cm^2 V^{-1} s^{-1} for **1** and **2**, respectively. The electron mobilities for both the active layers (estimated from the *J*–*V* characteristics of the electron only device shown in Fig. S14†) were almost the same for both **1** and **2***i.e.* 2.56×10^{-4} cm^2 V^{-1} s^{-1}, since the electron mobility is dominated by acceptor molecule ($PC_{71}BM$). Therefore the ratio between the electron and hole mobilities for the devices based on **1** and **2** are about 2.95 and 8.71, respectively, leading to the better charge transport in the device based on **1**, as compared to **2**, resulting higher values of J_{sc}, FF and PCE.

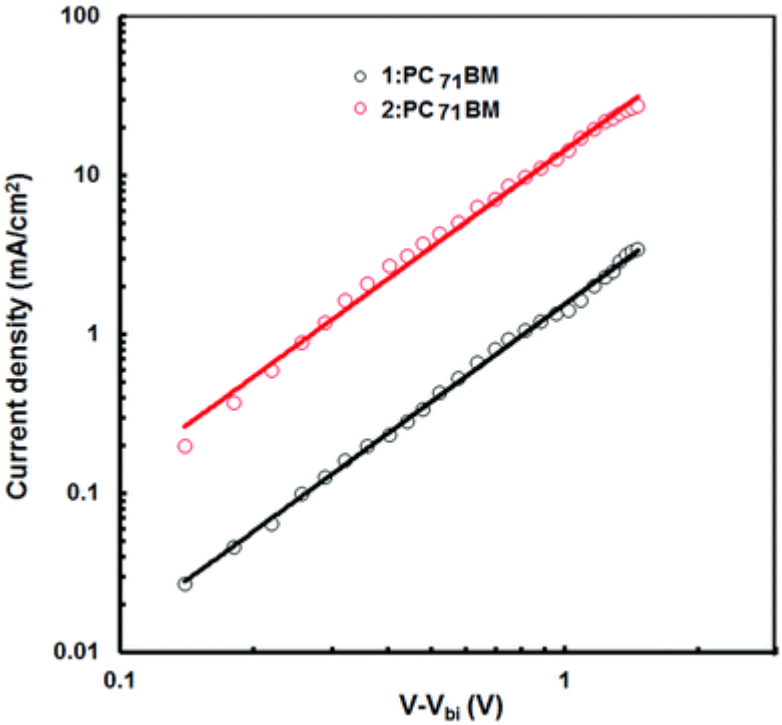

Fig. 11 Variation of dark current density with V–V_{bi} for hole only devices. The solid lines indicate fits of experimental data that yields a slope of 2.

To get information about the exciton generation and dissociation behaviors, in these solar cells based on **1** and **2**, we have evaluated the maximum photoinduced carrier generation rate per unit volume (G_{max}) and charge collection probability (P_c) in these devices. The devices were biased swept from −1 V to 1 V. Fig. 12 shows the variation of photocurrent (J_{ph}) with effective voltage (V_{eff}) for devices based on 1 and 2 small molecules, measured under illumination at 100 mW cm^{-2}. J_{ph} is defined as $J_{ph} = J_L - J_D$, where J_L and J_D are the current densities under illumination and in the dark. V_{eff} is defined as $V_{eff} = V_o - V_{app}$, V_o is the voltage, when $J_{ph} = 0$ ($J_L = J_D$), and V_{app} is the applied voltage.[71] Fig. 12 shows the two distinct regions: (i) J_{Ph}increases linearly at low V_{eff}, and (ii) J_{ph} is saturated at high V_{eff}, at which the internal electric field is large enough to dissociate all the photogenerated excitons into free charge carriers and sweep out all the carriers to the electrodes. Therefore, at high V_{eff}, the saturation photocurrent density ($J_{ph,sat}$) is limited by the total number of absorbed photons, and assuming that $J_{ph,sat}$ is independent of bias and temperature, we determined the G_{max}, using $J_{ph,sat} = qLG_{max}$, where q is the electronic charge and L is the thickness of the active layer used in the device.[72] The values of G_{max} for the devices based on **1** and **2** are 8.36 × 10^{27} m^{-3} s^{-1} ($J_{ph,sat}$ = 134 A m^{-2}) and 7.43 × 10^{27} m^{-3} s^{-1} ($J_{ph,sat}$ = 122 A m^{-2}), respectively. It is noted here that G_{max} is the maximum number of absorbed photons and such an enhancement corresponds to the increased light absorption in the device based on **1**, consistent with the absorption spectra of the **1**. The photocurrent density can be expressed as[73,74]

$$J_{ph}(V) = P_{in}\eta_A\eta_{ED}\eta_{CT}P_C(V),$$

where V is the applied voltage across the device, P_{in} is the incident light intensity, η_A is the absorption efficiency of photons in the active layer, η_{ED} is the exciton diffusion efficiency, which is the efficiency of photogenerated excitons diffusing to the D–A interfaces, η_{CT} is the charge transfer efficiency, which is related to the LUMO off-set between the donor and acceptor materials used in the BHJ active layer, and $P_C(V)$ is the charge collection efficiency, *i.e.* the probability of charge collection of the separated carriers. The charge collection probability is voltage dependent. The $P_c(V)$ can be expressed as[75]

$$P_C(V) = J_{ph}(V)/J_{ph,sat}$$

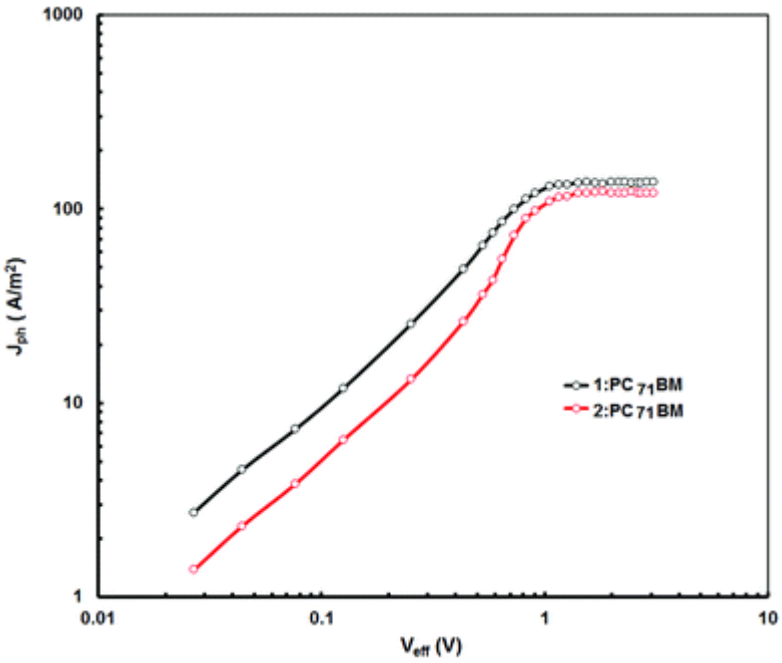

Fig. 12 Variation of photocurrent density (J_{ph}) as a function of effective voltage (V_{eff}) for the devices.

Under short circuit conditions, $P_C(0)$ is equal to $J_{sc}/J_{ph,sat}$, and the values of $P_C(0)$ for the device based on **1** and **2** are 0.89 and 0.83, respectively. The higher value of charge collection probability is attributed to the more favorable nanoscale morphology of the **1** : $PC_{71}BM$ active layer.

4. Conclusions

In summary, we have designed and synthesized two low band gap small molecules **DRT3-BDT (1)** and **DTT3-BDT (2)**, comprising the same BDT central core (donor) and different end capped acceptor units, *i.e.* rhodanine with ethyl hexyl and thiazolidione with ethylhexyl linked *via* an alkyl-substituted terthiophene (3 T) π-conjugation bridge, respectively, and used them as electron donors along with $PC_{71}BM$ as an electron acceptor for BHJ small molecule solar cells. These devices showed quite reasonable high V_{oc} values, attributed to their deeper HOMO energy levels. The optimized devices (processed with 3 v% DIO/CF), based on **1** : $PC_{71}BM$ and **2** : $PC_{71}BM$ active layers, yielded PCE values of 6.76% and 5.26%, respectively. The higher value of PCE for the former device has been attributed to the more appropriate nanoscale morphology of the active layer and balanced charge transport than the latter device.

Acknowledgements

EP would like to thank MINECO for the project CTQ2013-47183-R and the support through Severo Ochoa Excellence Accreditation 2014-2018(SEV-2013-0319). We also thankful to the Material Science laboratory, MNIT, Jaipur and Department of Physics, LNMIT, Jaipur for the availability of device fabrication facilities and other characterizations.

References

1 G. Dennler, M. C. Scharber and C. J. Brabec, Adv. Mater.,

2009, 21, 132.

2 P. M. Beaujuge and J. M. J. Fréchet, J. Am. Chem. Soc., 2011,

133, 20009.

3 G. Li, R. R. Zhu and Y. Yang, Nat. Photonics, 2012, 6, 153.

4 S. Günes, H. Neugebauer and N. S. Sariciftci, Chem. Rev.,

2007, 107, 1324.

5 A. Facchetti, Chem. Mater., 2011, 23, 733.

6 B. Walker, C. Kim and T.-Q. Nguyen, Chem. Mater., 2011,

23, 470.

7 J. Roncali, Acc. Chem. Res., 2009, 42, 1719.

8 G. Yu, J. Gao, J. C. Hummelen, F. Wudl and A. J. Heeger,

Science, 1995, 270, 1789.

9 Y. J. Cheng, S. H. Yang and C. S. Hsu, Chem. Rev., 2009,

109, 5868.

10 (a) F. C. Krebs, Sol. Energy Mater. Sol. Cells, 2009, 93, 394;

(b) T. D. Nielsen, C. Cruickshank, S. Foged, J. Thorsen and

F. C. Kreb, Sol. Energy Mater. Sol. Cells, 2010, 94, 1553.

11 H. Hoppe and N. S. Sariciftci, J. Mater. Chem., 2006, 16, 45.

12 M. Helgesen, R. Søndergaard and F. C. Krebs, J. Mater.

Chem., 2010, 20, 36.

13 W. Cao and J. Xue, Energy Environ. Sci., 2014, 7, 2123.

14 Z. C. He, C. M. Zhong, S. J. Su, M. Xu, H. B. Wu and Y. Cao,

Nat. Photonics, 2012, 6, 591.

15 W.-Y. Wong and C.-L. Ho, Acc. Chem. Res., 2010, 43, 1246.

16 Z. C. He, C. M. Zhong, X. Huang, W.-Y. Wong, H. B. Wu,

L. W. Chen, S. J. Su and Y. Cao, Adv. Mater., 2011, 23, 4636.

17 J. You, L. Dou, K. Yoshimura, T. Kato, K. Ohya, T. Moriarty,

K. Emery, C. C. Chen, J. Gao, G. Li and Y. Yang, Nat.

Commun., 2013, 4, 1446.

18 S. Liu, K. Zhang, J. Lu, J. Zhang, H.-L. Yip, F. Huang and

Y. Cao, J. Am. Chem. Soc., 2013, 135, 15326.

19 M. T. Lloyd, J. E. Anthony and G. G. Malliaras, Mater.

Today, 2007, 11, 34.

20 D. H. Wang, A. K. K. Kyaw, V. Gupta, G. C. Bazan and

A. J. Heeger, Adv. Energy Mater., 2013, 3, 1161.

21 J. Zhou, Y. Zuo, X. Wan, G. Long, Q. Zhang, W. Ni, Y. Liu,

Z. Li, G. He, C. Li, B. Kan, M. Li and Y. Chen, J. Am. Chem.

Soc., 2013, 135, 8484.

22 Y. Liu, C. Chen, Z. Hong, J. Gao, Y. M. Yang, H. Zhou,

L. Dou, G. Li and Y. Yang, Sci. Rep., 2013, 3, 3356.

23 Y. Chen, X. Wan and G. Long, Acc. Chem. Res., 2013, 46,

2645.

24 A. Mishra and P. Bauerle, Angew. Chem., Int. Ed., 2012, 51,

2020.

25 J. E. Coughlin, Z. B. Henson, G. C. Welch and G. C. Bazan,

Acc. Chem. Res., 2014, 47, 257.

26 Y. Lin, Y. Li and X. Zhan, Chem. Soc. Rev., 2012, 41, 4245.

27 A. K. K. Kyaw, D. H. Wang, D. Wynands, J. Zhang,

T. Q. Nguyen, G. C. Bazan and A. J. Heeger, Nano Lett.,

2013, 13, 3796.

28 B. Kan, Q. Zhang, M. Li, X. Wan, W. Ni, G. Long, Y. Wang,

X. Yang, H. Feng and Y. Chen, J. Am. Chem. Soc., 2014, 136,

15529.

29 Y. Liu, C. Chen, Z. Hong, J. Gao, Y. Yang, H. Zhou, L. Dou,

G. Li and Y. Yang, Sci. Rep., 2013, 3, 3356.

30 B. Walker, C. Kim and T. Q. Nguyen, Chem. Mater., 2011,

23, 470.

31 J. Min, Y. N. Luponosov, T. Ameri, A. Elschner,

S. M. Peregudova, D. Baran, T. Heumuller, N. Li, F. Machui,

S. Ponomarenko and C. J. Brabec, Org. Electron., 2013, 14,

219.

32 J. Min, Y. N. Luponosov, A. Gerl, M. S. Polinskaya,

S. M. Peregudova, P. V. Dmitryakov, A. V. Bakirov,

M. A. Shcherbina, S. N. Chvalun, S. Grigorian, N. K. Busies,

S. A. Ponomarenko, T. Ameri and C. J. Brabec, Adv. Energy

Mater., 2014, 4, 1301234.

33 J. Min, Y. N. Luponosov, Zhi-Guo Zhang,

S. A. Ponomarenko, T. Ameri, Y. Li and C. J. Brabec, Adv.

Energy Mater., 2014, 4, 1400816.

34 Y. Z. Lin, L. C. Ma, Y. F. Li, Y. Q. Liu, D. B. Zhu and

X. W. Zhan, Adv. Energy Mater., 2013, 3, 1166.

35 Y. M. Sun, G. C. Welch, W. L. Leong, C. J. Takacs,

G. C. Bazan and A. J. Heeger, Nat. Mater., 2012, 11, 44.

36 Y. S. Liu, Y. Yang, C. C. Chen, Q. Chen, L. T. Dou,

Z. R. Hong, G. Li and Y. Yang, Adv. Mater., 2013, 25, 4657.

37 J. Y. Zhou, X. J. Wan, Y. S. Liu, Y. Zou, Z. Li, G. R. He,

G. K. Long, W. Ni, C. X. Li, X. C. Su and Y. S. Chen, J. Am.

Chem. Soc., 2012, 134, 16345.

38 J. Min, Z. G. Zhang, S. Zhang and Y. Li, Chem. Mater., 2012,

24, 3247.

39 L. Dou, J. Gao, E. Richard, J. You, C. C. Chen, K. C. Cha, Y. He, G. Li and Y. Yang, J. Am. Chem. Soc., 2012, 134, 10071.

40 W. Li, W. S. Roelofs, M. M. Wienk and R. A. Janssen, J. Am. Chem. Soc., 2012, 134, 13787.

41 L. Huo, J. Hou, S. Zhang, H. Y. Chen and Y. Yang, Angew. Chem., Int. Ed., 2010, 49, 1500.

42 Z. Du, W. Chen, Y. Chen, S. Qiao, X. Bao, S. Wen, M. Sun, L. Han and R. Yang, J. Mater. Chem. A, 2014, 2, 15904.

43 Y. Huang, X. Guo, F. Liu, L. Huo, Y. Chen, T. P. Russell, C. C. Han, Y. Li and J. Hou, Adv. Mater., 2012, 24, 3383.

44 D. Lee, E. Hubijar, G. J. D. Kalaw and J. P. Ferraris, Chem. Mater., 2012, 24, 2534.

45 Y. Li, Acc. Chem. Res., 2012, 45, 723.

46 M. Zhang, Y. Gu, X. Guo, F. Liu, S. Zhang, L. Huo, T. P. Russell and J. Hou, Adv. Mater., 2013, 25, 4944.

47 J. Zhou, X. Wan, Y. Liu, Y. Zuo, Z. Li, G. He, G. Long, W. Ni, C. Li, X. Su and Y. Chen, J. Am. Chem. Soc., 2012, 134, 16345.

48 D. Patra, T. Y. Huang, C. C. Chiang, R. O. V. Maturana, C. W. Pao, K. C. Ho, K. H. Wei and C. W. Chu, ACS Appl. Mater. Interfaces, 2013, 5, 9494.

49 J. Zhou, X. Wan, Y. Liu, G. Long, F. Wang, Z. Li, Y. Zuo,

C. Li and Y. Chen, Chem. Mater., 2011, 23, 4666.

50 D. Ye, X. Li, L. Xan, W. Zhang, Z. Hu, Y. Liang, J. Fang,

W. Y. Wong and X. Wang, J. Mater. Chem. A, 2013, 1, 7622.

51 C. C. Patra, W. A. Chiang, K. H. Chen, M. C. Wei, M. C. Wu

and C. W. Chu, J. Mater. Chem. A, 2013, 1, 7767.

52 W. Ni, M. Li, X. Wan, H. Feng, B. Kan, Y. Zuo and Y. Chen,

RSC Adv., 2014, 4, 31977.

53 K. Sun, Z. Xiao, S. Lu, W. Zajaczkowski, W. Pisula,

E. Hanssen, J. M. White, R. M. Williamson, J. Subbiah,

J. Ouyang, A. B. Holmes, W. W. H. Wong and D. J. Jones,

Nat. Commun., 2015, 6, 6013, DOI: 10.1038/ncomms7103.

54 C. V. Kumar, L. Cabau, E. N. Koukaras, A. Viterisi,

G. D. Sharma and E. Palomares, J. Mater. Chem. A, 2015, 3,

4892.

55 J. P. Perdew, K. Burke and M. Ernzerhof, Phys. Rev. Lett.,

1996, 77, 3865.

56 A. Schafer, H. Horn and R. Ahlrichs, J. Chem. Phys., 1992,

97, 2571.

57 K. Eichkorn, Q. Treutler, H. Öhm, M. Häser and

R. Ahlrichs, Chem. Phys. Lett., 1995, 240, 283.

58 A. D. Becke, J. Chem. Phys., 1993, 98, 5648.

59 C. Lee, W. Yang and R. G. Parr, Phys. Rev. B: Condens.

Matter, 1988, 37, 785.

60 Y. Zhao and D. G. Truhlar, Theor. Chem. Acc., 2008, 120,

215.

61 M. J. Frisch, G. W. Trucks, H. B. Schlegel, G. E. Scuseria,

M. A. Robb, J. R. Cheeseman, G. Scalmani, V. Barone,

B. Mennucci, G. A. Petersson, H. Nakatsuji, M. Caricato,

X. Li, H. P. Hratchian, A. F. Izmaylov, J. Bloino, G. Zheng,

J. L. Sonnenberg, M. Hada, M. Ehara, K. Toyota, R. Fukuda,

J. Hasegawa, M. Ishida, T. Nakajima, Y. Honda, O. Kitao,

H. Nakai, T. Vreven, J. A. Montgomery, Jr., J. E. Peralta,

F. Ogliaro, M. Bearpark, J. J. Heyd, E. Brothers,

K. N. Kudin, V. N. Staroverov, R. Kobayashi, J. Normand,

K. Raghavachari, A. Rendell, J. C. Burant, S. S. Iyengar,

J. Tomasi, M. Cossi, N. Rega, J. M. Millam, M. Klene,

J. E. Knox, J. B. Cross, V. Bakken, C. Adamo, J. Jaramillo,

R. Gomperts, R. E. Stratmann, O. Yazyev, A. J. Austin,

R. Cammi, C. Pomelli, J. W. Ochterski, R. L. Martin,

K. Morokuma, V. G. Zakrzewski, G. A. Voth, P. Salvador,

J. J. Dannenberg, S. Dapprich, A. D. Daniels, Ö. Farkas,

J. B. Foresman, J. V. Ortiz, J. Cioslowski and D. J. Fox, Gaussian

03, revision C.01, Gaussian, Inc., Wallingford CT, 2004.

62 TURBOMOLE (version 5.6), Universität Karlsruhe, 2000.

63 D. Jacquemin, E. A. Perpète, I. Ciofini, R. Adamo Valero,

Y. Zhao and D. G. Truhlar, J. Chem. Theory Comput., 2010,

6, 2071.

64 S. Mathew, A. Yella, P. Gao, R. Humphry-Baker,

F. E. Curchod, N. Ashari-Astani, I. Tavernelli,

U. Rothlisberger, M. K. Nazeeruddin and M. Grätzel, Nat.

Chem., 2014, 6, 242.

65 N. Lim, N. Cho, S. Paek, C. Kim, J. K. Lee and J. Ko, Chem.

Mater., 2014, 26, 2283.

66 X. N. Yang, J. Loos, S. C. Veenstra, W. J. H. Verhees,

M. M. Wienk, J. M. Kroon, M. A. J. Michels and

R. A. J. Janssen, Nano Lett., 2005, 5, 579.

67 J. E. Slota, X. He and W. T. S. Huck, Nano Today, 2010, 5,

231.

68 J. Peet, M. L. Senatore, A. J. Heeger and G. C. Bazan, Adv.

Mater., 2009, 21, 1521.

69 K. Schmidt, C. J. Tossone, J. R. Niskala, A. T. Yiu, O. P. Lee,

T. M. Weiss, C. Wang, J. M. J. Fré chet, P. M. Beaujuge and

M. F. Toney, Adv. Mater., 2014, 26, 300.

70 D. H. Kim, A. L. Ayzner, A. L. Appleton, K. Schmidt,

J. G. Mei, M. F. Toney and Z. A. Bao, Chem. Mater., 2013,

25, 431.

71 S. R. Cowan, A. Roy and A. J. Heeger, Phys. Rev. B: Condens.

Matter Mater. Phys., 2010, 82, 245207.

72 V. D. Mihailetchi, H. X. Xie, B. de Boer, L. J. A. Koster and

P. W. M. Blom, Adv. Funct. Mater., 2006, 16, 699.

73 R. A. Street, A. Krakaris and S. R. Cowan, Adv. Funct. Mater.,

2012, 22, 4608.

74 Z. He, C. Zhong, X. Huang, W.-Y. Wong, H. Wu, L. Chen,

S. Su and Y. Cao, Adv. Mater., 2011, 23, 4636.

75 Z. Yi, W. Ni, Q. Zhang, M. Li, B. Kan, X. Wan and Y. Chen,

J. Mater. Chem. C, 2014, 2, 7247.